NTNU – Trondheim
Norwegian University of
Science and Technology

Monte Carlo Simulations of a simple Model for Charge Storage in a Single-file Nanopore

Endre Skeie

Master of Science in Physics and Mathematics
Submission date: June 2015
Supervisor: Peter Berg, IFY

Norwegian University of Science and Technology
Department of Physics

Preface

This Master's thesis is the final part of the Master of Science program in Applied Physics and Mathematics at the Norwegian University of Science and Technology. The thesis is equivalent to one semester's work and was written from January to June 2015. It was written at the Department of Physics under the supervision of Professor Peter Berg.

Acknowledgement

I would like to thank my supervisor Professor Peter Berg for the fruitful discussions and valuable guidance during the Master's thesis. I would also like to thank Vincent Démery for answering my questions regarding his previous work.

Abstract

This Master's thesis is focusing on charge storage in a nanopore inside an electrode. It introduces a simple model where the only present interactions are electrostatic and steric effects, which allows only one ion to be at a lattice point. The nanopore modelled is a defect nanopore, where only the end of the pore interior has the potential of an electrode. Monte Carlo simulations are used for studying the behaviour of the model. Interesting behaviours found in the model are overscreening, charge density oscillations and oscillating differential capacitance as a function of the imposed charge, which all disappear at high temperatures. If the electrolyte is a filled ionic liquid, the differential capacitance curves are found to have camel-shape. When the electrolyte is diluted, the peaks of the oscillating differential capacitance are shifted and at the point of zero charge the differential capacitance has a bell-shape. These findings are the opposite of a system when the ions are not confined, studied previously as a flat capacitor by Démery *et al.*

Sammendrag

Denne masteroppgaven omhandler elektrisk lagring i en pore på størrelsen av et ion i en kondensator. Den introduserer en enkel modell, hvor de eneste kreftene er elektrostatiske i tillegg til steriske effekter som begrenser at kun et ion kan være på et gitterpunkt. Poren som blir laget modell av er en defekt pore, hvor bare innerste delen av poren er på samme potensial som elektroden. Monte Carlo simuleringer er brukt for å beskrive egenskapene til modellen. De interessante egenskaper til modellen er over-skjerming, oscillerende ladningstetthet langs poren og oscillerende kapasitans som funksjon av ladning ved elektrodene, som alle forsvinner ved høy temperatur. Hvis elektrolytten er en fylt ionisk væske, stiger kapasitansen med økende ladning ved elektrodene rundt null ladning ved elektrodene. Hvis elektrolytten fjerner ione-par, endrer lokasjonen til topp-punktene til den oscillerende kapasitansen seg. Og rundt null ladning ved elektrodene, synker kapasitansen med økende ladning ved elektrodene. Disse funnene er motsatt av når ionene kan bevege seg fritt, studert som en flat kondensator av Démery *et al.*

Contents

List of Figures

List of Tables

Physical Variables and Natural Constants

Table 1: Variables and natural constants used in this thesis.

Name	Variable	Numerical value	SI Units
Vacuum permittivity	ε_0	8.85419×10^{-12}	F m^{-1}
Relative permittivity	ε_r		
Boltzmann's constant	k_B	1.38065×10^{-23}	J K^{-1}
Temperature	T		K
Distance	r		m
Charge of ions	q	1.60218×10^{-19}	C
Diameter	d		m
Energy	E		J
Surface charge density	σ		C m^{-2}
Potential	u		V
Interaction parameter	γ		
Imposed charge	Q		
System size	M		
Potential difference	Δu		
Differential capacitance	c		
Filling factor	μ		
Scaling of extra ion-ion correlation	f		
Screening factor	s		
Probability	p		
Number of states	N_s		

Continued on next page

Table 1 – *Continued from previous page*

Name	Variable	Numerical value	SI Units
Monte Carlo time steps	N		
Monte Carlo relaxation steps	K		

Chapter 1

Introduction

This thesis is focused upon a simple model for charge storage in a nanopore capacitor, where its behaviour is presented with Monte Carlo simulations.

1.1 Background

Storing electrical energy is a bottleneck of technology which limits technical development. An more effective way to store electrical energy would help the transformation form a hydrocarbon-fueled society to a low carbon one. For example, electricity generated from renewable energy sources such as solar and wind can have large variations in the power output [5]. Storing some of the energy from peak hours and delivering it later, would greatly improve the stability of these sources. Batteries have mostly been used in electrical energy storage the last century, due to their energy density and relatively cheap production costs. However, their power density and cycle lifetime are limited. Recent research has shown promising results to improve these limitations of batteries [6].

Supercapacitors, also called electric double layer capacitors or electrochemical capacitors, have high power density and impressive cycle lifetime, but have moderate energy density [7, 8]. These store energy by attracting ions to counterbalance the surface charge of an electrode. Supercapacitors have high power density and

cycle lifetime because the charge cycle does not involve chemical reactions. In order to improve supercapacitors one must predict the electro-chemical flow, which is highly influenced by the interface of the electrolyte and the charged electrode. A phenomenon occurring at the interface which is not yet completely understood, is the electric double layer.

1.1.1 Electric Double Layer

The electric double layer is formed because the surface charge attracts ions of opposite charge in the electrolyte and a layer of these so-called co-ions is formed next to the surface, hence the name. Figure 1.1 shows a schematic of the interface between a negatively charged surface and an electrolyte. Ever since Helmholtz's first model of the interface between an electrolyte and a charged solid [9] assumed the presence of a compact layer of ions in contact of the charged surface, scientists have tried to model the phenomena. The next step forward came from a model by Gouy and Chapman, who introduced a diffuse double layer which extended to some distance from the surface due to the Boltzmann distribution. A problem with this model was that the distance between the surface and the solution-phase charge zones decreased towards zero for high charge densities. A modification by Stern removed the singularity by introducing a minimum distance between the phases. Even though these models are almost a century old, they still have an impact more modern models.

In more recent times, modified Poisson-Boltzmann equations are used to model the electric double layer [10]. These mean-field models predicts the formation of the electric double layer where the ions are loosely bound to the surface. At small surface charge densities, the models qualitatively explain experimental results. However, the models fail to describe the electric double layer as the surface charge

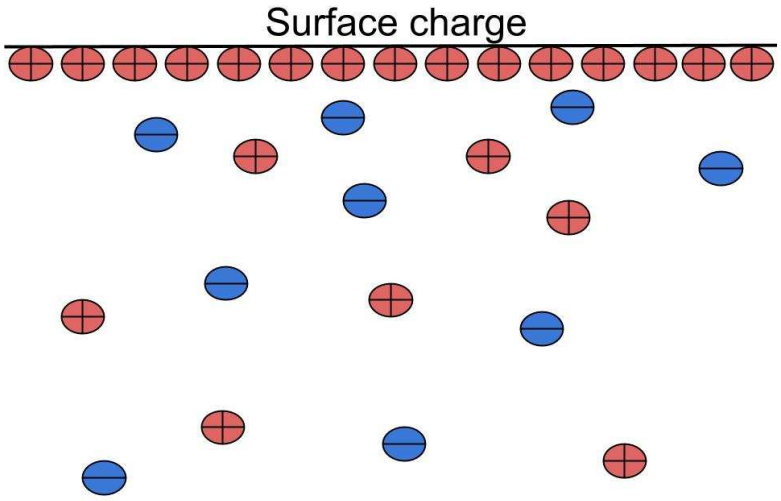

Figure 1.1: Schematic of the electric double layer with negative surface charge, where solvent molecules are not drawn.

densities and the valency of the co-ions increase [11].

1.1.2 Ionic Liquid

Another way to improve the performance of the supercapacitors is to use electrolytes with fitting properties. The internal resistance and operation voltage are mostly determined by the properties of the electrolytes. Ionic liquids are salts whose ions are so large that their electrostatic interaction is small enough to remain in the liquid state at room temperatures. They are solvent-free electrolytes, which makes them well suited for applications requiring a high concentration of ionic charge, such as in supercapacitors [12]. Additional desirable properties are high thermal and chemical stability, low vapour pressure and low flammability [13, 14]. The interest of this research topic has grown along with the interest of supercapacitors.

1.1.3 Nanopores

There are two ways to increase the energy density of supercapacitors, increasing interfacial area per volume or increase the double layer capacitance per unit surface area. To increase the interfacial area per volume, porous electrodes are used [15]. Carbon based porous electrodes are often used because of their low cost, high electric conductivity and stability [16]. The carbon electrodes can have different forms and properties depending on source materials, forming process and forming conditions. The electrodes become a three-dimensional network of nanopores with various sizes.

A significant increase in the capacitance has been observed experimentally when the pore sizes approached the size of an ion, indicating a different behaviour of the capacitance when the ions can not move freely [1, 17, 18]. Figure 1.2 shows the results from reference [1]. These findings was later confirmed with classical density functional theory [19], and molecular dynamics [20, 21].

1.2 Previous Work

A formally, exactly solvable model for a flat ionic liquid capacitor has been studied by Démery *et al.* [3].Here the authors introduced the one-dimensional Coulomb lattice fluid capacitor, where the system interacts as sheets of charge density fixed at the lattice points. On both ends, the electrodes are represented by imposing a positive and negative charge density or a potential drop between them. The sheets in the electrolyte can swap location, and the steric effect by restricting the maximal occupancy at any lattice site to one sheet. This model predicted results not found in mean-field models, such as strong oscillations in capacitance as a function of applied voltage. The analytical results were confirmed with Monte

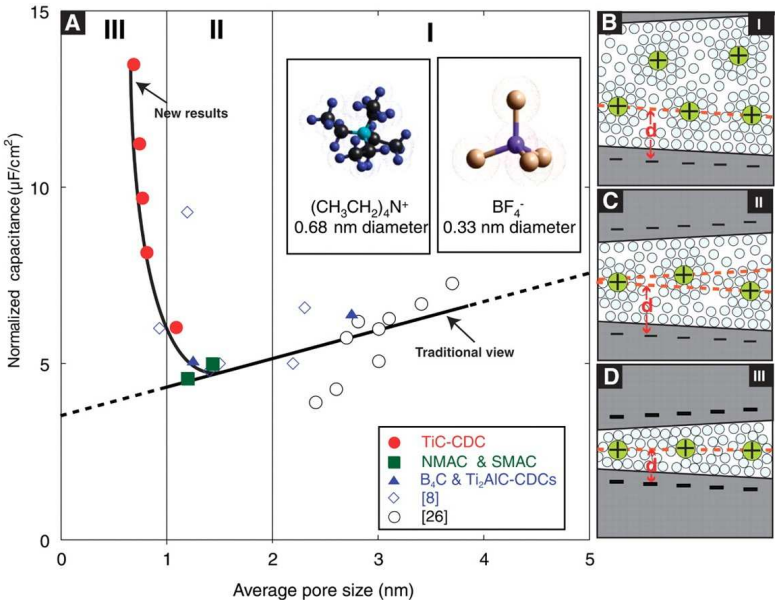

Figure 1.2: (A) Plot of specific capacitance for three different studies using identical electrolytes. Insets are the sketch of organic electrolyte molecular used in the experiments. (B to D) Schematic of solvated ions with distance between adjacent pore walls (B) greater than 2 nm, (C) between 1 and 2 nm, and (D) less than 1 nm. From ref. [1]. Reprinted with permission from AAAS. Link

Carlo simulations.

The observations of the different behaviour of the capacitance as pore size decreases, such seen in figure 1.2, have sparked a great interest in understanding the charge storage in supercapacitors. The first to publish theoretical work on this behaviour were Huang *et al.* in 2008 [22, 2]. The authors proposed a heuristic theoretical model based on the traditional parallel-plate capacitor which takes the pore curvature into account. In the macropore regime ($> 50\ nm$) the pore curvature is no longer significant and the model is reduced to the classical Helmholtz model. For mesopores ($2 - 50\ nm$), assuming cylindrical pores, the counter-ions tend towards the surface and form a double cylindrical capacitor along with the pore. For micropores ($< 2\ nm$), the pore size prevents formation of a double cylin-

drical capacitor. The authors assumed instead that the counter-ions line up in the pore to form an electric wire in a cylinder capacitor. Figure 1.3 shows a schematic of of ions in negatively charged mesopores and micropores. The authors showed that their model can match experimental data of capacitance in nanopores, giving an explanation for the behaviour of increasing capacitance as pore size decreases.

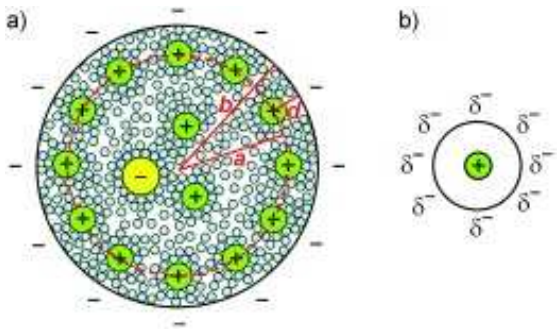

Figure 1.3: Schematic diagrams of a) a negatively charged mesopore creating a double cylindrical capacitor with the solvated cations, and b) a negatively charge micropore forming an electric wire in a cylinder capacitor with the cations. Reprinted with permission from ref. [2]. Copyright 2008, John Wiley and Sons. Link

The capacitance of the double layer formed at a metal and ionic liquid interface can be remarkably large, which mean-field theories fail to explain. Skinner *et al.* [23] proposed an alternative theory, which allowed the binding between discrete ions and their image charge in the metal. Hence demonstrated the capacitance can be larger than predicted by the Helmholtz model. In 2011 [24], the authors extended their model from the planar electrode to narrow pores with high interfacial area per volume. They showed that for ions confined within narrow pores, the ions induced an infinite row of image charges going into the pore, which screened the ions. At low ion densities, capacitance increases as voltage and pore size decreases. The authors presumed that as the pore size decreases, the screening of ions increases and therefore also the capacitance. The opposite

was presumed for imperfect metals with limited screening effects, hence giving a larger effective pore size. As for decreasing voltage fewer ions will be inside the pore, causing a decrease in ion-ion interaction and giving higher capacitance.

The screening of the ions seems to be the reason for the high capacitance of nanopore capacitors. Lee *et al.* [25] introduce an exactly solvable one-dimensional lattice model for charging a nanopore. The model takes into account the exponential screening of ion-ion interaction by introducing a "super-ionic" state explained in [26]. The ion-ion interaction is approximated to a nearest neighbour interaction. The analytical expressions describe the mechanism of charge storage and the qualitative form of the capacitance. The capacitance is sensitive to how favourable it is for ions to occupy the neutral pore as well as the pore radius. At zero voltage the capacitance increases with decreasing pore size, in agreement with experimental observations. The authors consider the electrode to be a metallic conductor, screening the ions. However, some porous electrodes in use today are not perfect metallic conductors. In addition, the screening ions are spread along the electrode in a mean-field like way, not following the respective ions in the liquid.

These studies of charge storage in nanopores assume equilibrium or infinitely slow charging. In practice, the capacitors operate with fast charging and discharging. Simulations with molecular dynamics studying the cyclic charging behaviour [27] and time dependence of charging [28] have been conducted for a single nanopore. As our work assumes equilibrium conditions the findings of these papers are not so relevant, but are worth mentioning for a more complete understanding of charge storage with capacitors.

1.3 Goal of Thesis

The goal of this thesis is to create a simple model for charge storage in a nanopore. With this model we try to match the qualitative behaviour of the differential capacitance curves of experimental data and more complex models and simulations.

1.4 Thesis Outline

Following this introduction, the one-dimensional lattice model is introduced in chapter 2 along with a method to simulate the model for different conditions. Chapter 3 presents the results of the simulations. In chapter 4 the results are discussed in the context of experimental data and existing literature. In the end, a conclusion is drawn along with an outlook for further work.

Chapter 2

Model and Method

This chapter describes the model and the method used to simulate it.

2.1 The One-Dimensional Lattice Model

The following model is inspired by the exactly solvable one-dimensional model of a three-dimensional ionic liquid capacitor [3] and the single-file charge storage paper [25]. Here we consider a one-dimensional ionic liquid confined inside a pore that is an insulator. The model mirrors the pore, making it anti-symmetric. An illustration of the model is shown in Figure 2.1.

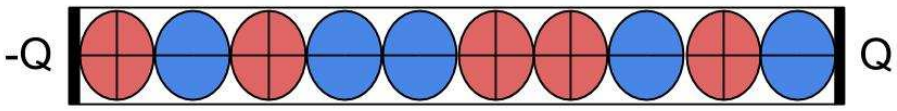

Figure 2.1: Schematic of the one-dimensional lattice model of the ionic liquid.

At both ends of the pore there are electrodes, represented in the model as opposite point charges placed at the electrodes. They are placed at a distance of half a diameter from the centre of the closest ions. The pore diameter is the same as the diameter of the ions. The electrolyte is densely packed as an ionic liquid

and it is assumed that the ions are hard spheres with the charge located at the centre of the ion. The steric effects are represented in the model by keeping the ions on fixed lattice points. It is assumed that the ions are monovalent, of same size and can swap locations. The model is electroneutral and it is assumed that the only interacting force is electrostatic, giving the following potential energy of two particles i and j

$$E_{ij} = \frac{1}{4\pi\epsilon_r\epsilon_0}\frac{q_i q_j}{r_{ij}}, \tag{2.1}$$

where ϵ_r and ϵ_0 are the relative and vacuum electric permittivity respectively, q_i and q_j are the charges of the corresponding particles and r_{ij} is the distance between them. When imposing charges at the electrodes, the one to the right is positive while the left one is negative. This will keep the model electroneutral, provided the electrolyte is electroneutral. The electroneutral set-up is chosen as we focus on a system of finite size M.

We introduce the dimensionless interaction parameter

$$\gamma = \frac{1}{4\pi\epsilon_r\epsilon_0 d}\frac{q^2}{k_b T}, \tag{2.2}$$

where d is the diameter of an ion, k_b is the Boltzmann factor, T is the temperature and q is the charge of an electron. The reason for introducing this parameter is explained in section 2.2. γ is the ratio of the electrostatic energy between two ions at neighbouring sites and the thermal energy $k_b T$. The potential energy of two particles i and j can then be written as

$$E_{ij} = \gamma\frac{Q_i Q_j}{R_{ij}}k_b T, \tag{2.3}$$

where Q_i and Q_j are the dimensionless charges of ion i and j respectively and R_{ij}

is the dimensionless distance between the ions.

An experimentally measurable quantity for a supercapacitor is the differential capacitance

$$c = \frac{d\sigma}{du}, \tag{2.4}$$

where σ is the surface charge density on the electrode and u is the potential. For this model where we impose the charge on the electrodes, we define our differential capacitance to be the dimensionless

$$c = \frac{dQ}{d\Delta u} = \frac{1}{\frac{d\Delta u}{dQ}}, \tag{2.5}$$

where Δu is the dimensionless potential difference between the electrodes and Q is the dimensionless imposed charge. The potential difference is the difference between the dimensionless potential created by the electrolyte at the electrodes. The dimensionless potential created by ion i at location j is $\frac{Q_i}{R_{ij}}$. By simulating the model at different values of the imposed charge Q, one can calculate the differential capacitance by the central difference approximation.

An alternative method to calculate the differential capacitance would be to obtain a continuous charge distribution by fitting splines of the discrete charge densities with a constraint on charge conservation. Such spline fitting with integral constraint is explained in reference [29]. One could then calculate the potential created by the electrolyte with Poisson's equation [9]. This method is not used because the spline fitting is expected to have significant error, which will be enhanced when solving Poisson's equation.

2.1.1 Modifications of the Model

Different modifications have been done for the model. In section 3.5 the effects of replacing ion pairs with voids or solvent, which still occupies space, are shown. This can be seen as the transition from an ionic liquid to a more dilute electrolyte. We introduce the filling factor μ. It describes how packed the pore is, that is the ratio of the number of ions to the number of lattice points.

The authors Storey *et al.* and Bazant *et al.* [30, 31] introduce an additional term to their free energy to enhance curvature of the mean electrostatic potential. This was included to give the mean field models an approximation of discrete interactions near the surface and the ability to describe overscreening. Although the one-dimensional lattice model already has steric effects and ion to ion Coulomb correlations, it would be interesting to evaluate what effect it would have to include an extra energy term which favours like or different ions to neighbours. The additional energy term of ion i and its neighbour

$$E_{i,i+1} = \gamma f Q_i Q_{i+1} k_b T \tag{2.6}$$

is included, where f is the scaling of the energy term. f is negative when favouring same charged ions to group together and different charged ions to group together when positive. Section 3.6 illustrates the effect of this energy term.

If the pore surrounding the ions is treated more realistically as a dielectric medium or a metal, charge carriers inside the pore would be attracted by the ions and partly screen the ions. For the model, one could therefore postulate that the induced pore charges near an ion are smeared out uniformly around such an ion. We introduce the screening factor s, ranging from zero (insulator) to one (metal). For s equals one, the potential along the centre of the pore created by an ion i

and its screening charge carriers becomes

$$u = \frac{q_i}{4\pi\epsilon_r\epsilon_0}\left(\frac{1}{r} - \frac{s}{\sqrt{r^2 + (d/2)^2}}\right). \tag{2.7}$$

By simplifying the expression in the parentheses it becomes

$$\frac{1}{r} - \frac{1}{\sqrt{r^2 + (d/2)^2}} = \frac{1}{r}\left(1 - \frac{1}{\sqrt{1 + (d/2r)^2}}\right). \tag{2.8}$$

Introducing $x = (d/2r)$ and expanding fraction gives

$$\frac{1}{r}\left(1 - \frac{1}{\sqrt{1 + (x)^2}}\right) = \frac{1}{r}\left(\frac{\sqrt{1 + (x)^2} - 1}{\sqrt{1 + (x)^2}}\right). \tag{2.9}$$

By taking the Taylor series of $\sqrt{1 + (x)^2}$ to the first order for $x \to 0$ the expression approximates to

$$\frac{1}{r}\left(\frac{\sqrt{1 + (x)^2} - 1}{\sqrt{1 + (x)^2}}\right) \approx \frac{x^2}{2r} = \frac{d^2}{8r^3}. \tag{2.10}$$

The potential scales like $1/r^3$ along the centre of the pore for r much larger than the pore diameter, weaker than for a point charge $(1/r)$ and a classical dipole $(1/r^2)$. For $s < 1$ the potential scales like a point charge, but with a reduced effective charge.

For computational purposes, we model the induced charges as two point charges with charge $qs/2$ on opposite sides of the ion. The potential created along the centre of the pore still is the same as equation (2.7), but the interaction between the induced charge carriers will differ. Figure 2.2 illustrates the approximation. Section 3.7 contains the results of this modification of the model.

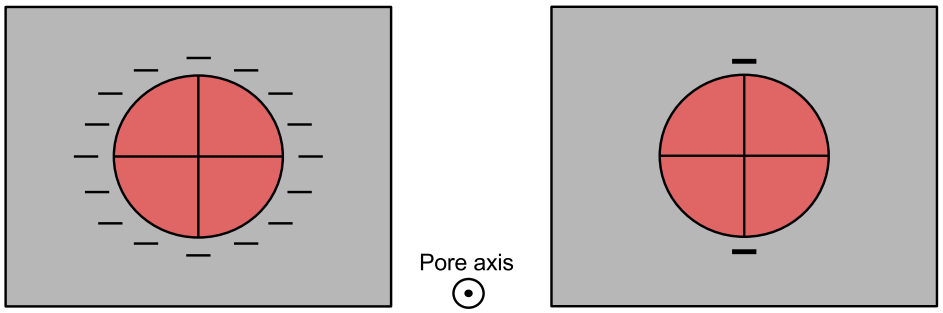

Figure 2.2: Illustration of the approximation from a smeared ring to two point charges.

2.2 Sampling the Model

The model is in contact with a heat bath with a temperature T. Treating the particles classically, the system follows the canonical ensemble [32]. This gives a probability for the system to be in state n according to

$$p(n) = \frac{e^{-\frac{E_n}{k_b T}}}{\sum_m e^{-\frac{E_m}{k_b T}}}, \tag{2.11}$$

where k_b is the Boltzmann factor and m sums over all states. From this one can easily calculate the average properties of the system by

$$\bar{A} = \sum_n p(n) A(n). \tag{2.12}$$

However, if the number of particles grows too large, a problem occurs, because the number of states becomes

$$N_s = \frac{M!}{(M/2)!(M/2)!}, \tag{2.13}$$

where M is the number of lattice points. For forty lattice points, the number of states becomes $\mathcal{O}(10^{11})$.

Instead of sampling all these states, it would be more convenient to sample a subset of states which represents the average distribution. A method to achieve this is the importance-sampling technique using the Metropolis algorithm [33]. The algorithm creates a Markov Monte Carlo chain, where the probability to go from state a to b is

$$p_{ab} = min(1, e^{-\Delta E/k_b T}), \tag{2.14}$$

where ΔE is the change in energy from state a to b. One can then calculate the average properties of the system by averaging over the sampled subset states. For more details, see appendix A. Because of the transition probability in equation (2.14), it is convenient to calculate the potential energy of two particles with equation (2.3), which is the reason for the usage of the parameter γ.

2.2.1 Sampling Algorithm

One initialises the model with the number of lattice points, number of ion pairs, screening factor s and interaction parameter γ. Then the ions are given a random configuration. To go from one state to another, two lattice points are randomly selected and the change of energy is calculated if the two ions were to swap locations. The probability for a swap is calculated with equation (2.14). A pseudo random number between zero and one is calculated and compared with the probability of changing the state. If the pseudo number is lower than the calculated probability, the two ions swap locations. One Monte Carlo time step is complete

when M attempts of changing the state have been made. As the two lattice points are randomly selected, during one Monte Carlo time step some sites may have been selected multiple times, while others were not. On average, each site is given the chance to swap twice.

In order for the importance sampling to be successful, three requirements must be met [34]. The first is that in a Markov chain, the next state of the system only depends on the preceding state and not on the history of the system. The Metropolis algorithm fulfils this requirement as the new state configuration and probability is calculated considering only the previous state. The second requirement is that the system is ergodic, which is that the properties of the system averaged over time is the same as averaged over the phase space of the system. For this system, the condition is fulfilled if all possible states are attainable. Although the system has states with different probabilities, each state is attainable as no state has infinite potential energy. The last requirement is the condition of detailed balance. Detailed balance implies that the number of times the system changes from state A to state B is equal to the number of times state B changes to state A. The transition probability in equation (2.14) fulfils this requirement in the Metropolis algorithm, as long as the states are Boltzmann distributed.

Before the sampling starts, the system is relaxed towards a lower energy, as the random configuration at start can be in a highly unlikely state. After the relaxation of the system, the sampling starts. For each Monte Carlo time step, the ion configuration and the potential difference between electrodes are logged. After the simulation is complete, the data is written to a text file. The simulations have been done in the programming language C++ with the Mersenne Twister random number generator, while Matlab has been used for post-processing the data. During this work, the efficiency of the code has been improved. At first,

the simulations were conducted on a personal computer, but to minimise the calculation time a server at Norwegian University of Science and Technology were used. The advantage of using the server was that one could run several simulations at the same time. For ten simulations with $M = 20$, 10^4 Monte Carlo time steps for relaxation (K), 10^5 Monte Carlo time steps for sampling (N) and imposed charges (Q) ranging from 0 to 10 with spacing of 0.05, the simulations took several hours.

Chapter 3

Results

In this chapter, all the results are presented.

3.1 Convergence of Simulations

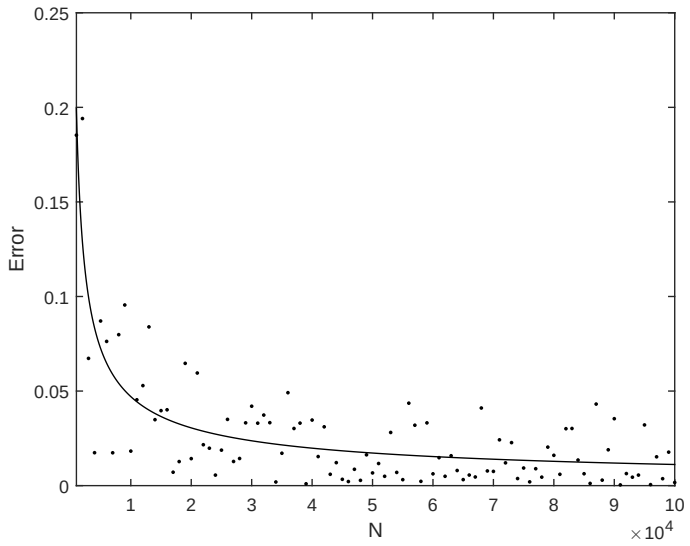

Figure 3.1: Error of Monte Carlo simulations as a function of number of Monte Carlo time steps (N) for $Q = 0$, $\gamma = 1$ and $K = 10^4$. The solid line is a fitted line of the points.

To study how the Monte Carlo simulations perform, the system was scaled down to 8 ions. One could then sample every state and calculate the exact prop-

erties with equation (2.11) and equation (2.12). The same system was then simulated with the Monte Carlo algorithm and the values of Δu were compared. This was done for different values of interaction parameter γ and imposed charge Q. At large γ and Q values, the Monte Carlo algorithm performed better than at smaller values. This is because the system becomes more bound, making the subset of important states smaller and easier to sample for the algorithm. With these findings, one scaled up the system and studied the "worst case scenario" used in the results. This was for M, Q and γ being respectively twenty, zero and one. Conveniently for Q being zero, the correct potential difference is then known to be zero as well. The difference between the exact value and the result of the Monte Carlo simulation as function of number of Monte Carlo steps are shown in figure 3.1. The fitted line in the figure are fitted as bN^m, where $b = 14.79$ and $m = -0.6243$.

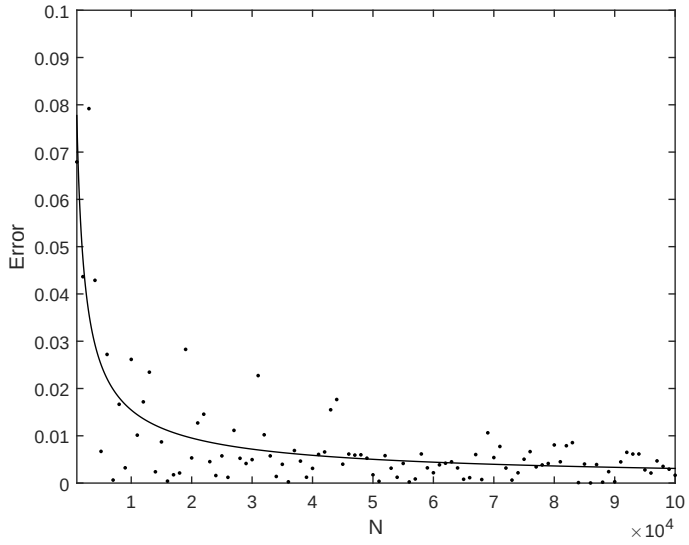

Figure 3.2: Error of average over ten Monte Carlo simulations as a function of number of Monte Carlo time steps for $Q = 0$, $\gamma = 1$ and $K = 10^4$. The solid line is a fitted line of the points.

By averaging over ten such simulations, the simulations performed as shown on figure 3.2. This method performed better than the individual simulations at cost of more computational time. The fitted line in this figure had the parameters $b = 9.592$ and $m = -0.6982$. All of the following results have been computed by averaging over ten simulations with 10^5 Monte Carlo time steps, 10^4 Monte Carlo relaxation steps and system size being 20. There was no observed change in the qualitative results when the system size was increased to 40 and 100.

3.2 Over-screening

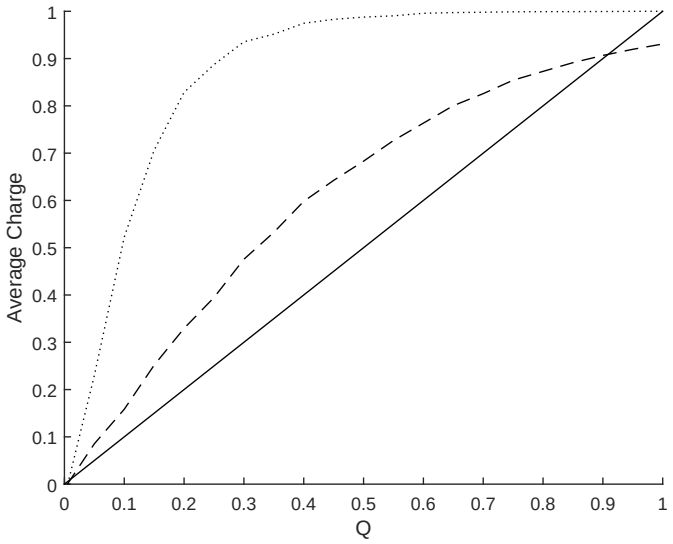

Figure 3.3: Average charge at the first lattice point as a function of imposed charge for $\gamma = 1$ (dashed) and 3 (dotted). The solid line is to visualise the absolute value of the imposed charge.

The phenomenon of over-screening can be seen in figure 3.3. The charge at the first lattice point can be higher than the imposed charge at the boundary, thus over-screening it. As the interaction parameter γ increases, that is as temperature

lowers, the over-screening becomes more prominent. Even at a relatively low imposed charge, one can reach saturation at the first lattice point, keeping the ion there.

3.3 Charge Density Oscillations

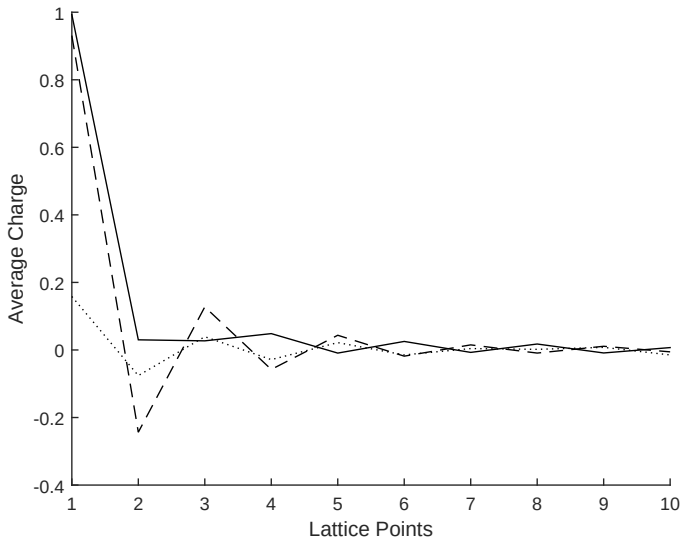

Figure 3.4: Charge oscillations along the lattice for $\gamma = 1$ and Q equals 1.7 (solid), 1 (dashed) and 0.1 (dotted).

Along with the over-screening, comes charge density oscillations. As the first ion over-screens the imposed charge, the second ion is attracted to the first ion. The third ion is then attracted to the second, and this continues into the electrolyte. Since the sites can be saturated, the charge density oscillations change while increasing the imposed charge. At first the ion over-screens the imposed charge, then the first ion becomes saturated. From this moment, charge oscillations decrease in amplitude as the imposed charge increases. This continues until

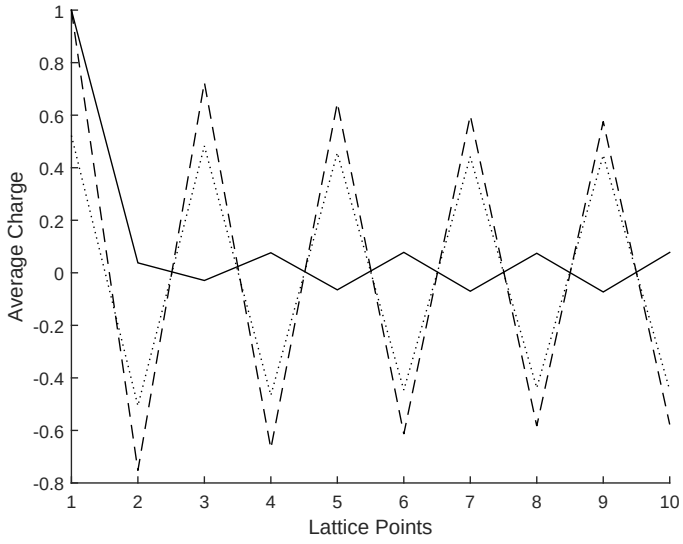

Figure 3.5: Charge oscillations along the lattice for $\gamma = 3$ and Q equals 1.7 (solid), 1 (dashed) and 0.1 (dotted).

the first ion perfectly screens the imposed charge and average charge is zero for the rest of the lattice point (except in the mirrored first ion). Then, as imposed charge increases, the second ion starts to screen the imposed charge and the first ion. The charge density oscillations increases until the two ions are saturated and in this way it continues in cycles as the imposed charge is further increased. Similar to the over-screening, the charge oscillations increase as γ increases. Figure 3.4 shows charge density oscillations for γ being 1 and figure 3.5 for γ being 3, at three different imposed charges. The imposed charge is located at lattice point 0.5.

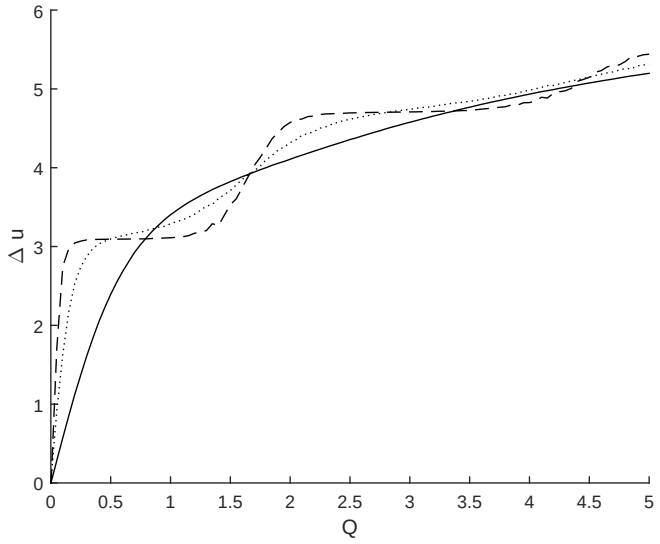

Figure 3.6: Potential difference between the walls as a function of the imposed charge for $\gamma = 1$ (solid), 3 (dotted) and 5 (dashed).

3.4 Temperature Dependence

Figure 3.6 shows the potential difference between the boundaries as a function of the imposed charge at the boundaries. As the temperature is lowered, plateau-like features emerge. These plateaus have a huge impact on the differential capacitance, changing the features completely, as seen in figure 3.7. The peaks keep increasing in height as the interaction parameter γ increases. At these temperatures, the first lattice point quickly screens the imposed charge. As the imposed charge increases, it is still over-screened and does not strongly attract opposite charged ions. This continues until the imposed charge is high enough to strongly attract another ion and saturates the lattice point. This results in repeating peaks in the differential capacitance curves.

As the differential capacitance is the inverse of the derivative of figure 3.6, it

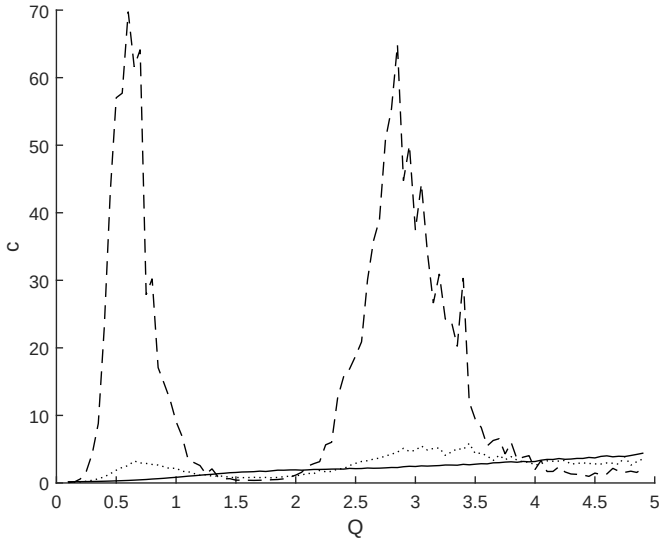

Figure 3.7: Differential capacitance as a function of the imposed charge for $\gamma = 1$ (solid), 3 (dotted) and 5 (dashed).

is very sensitive to small fluctuations of the Monte Carlo simulation, hence the spiky nature of the peaks in figure 3.7. At very high temperatures the peaks are not present and the differential capacitance has a nearly linear behaviour. The potential difference for γ equals five keeps oscillating around the higher temperature curve, with increasing width of plateaus, as the imposed charge is increased further than visualised in the figures. Therefore, the same is then seen in the differential capacitance, with increasing width of the peaks.

3.5 Effect of Voids

The effect of replacing ion pairs with voids is shown on figure 3.8. Removing just one pair from the ionic liquid softens the plateaus, yielding a similar effect as increasing the temperature described in the previous section. However, removing

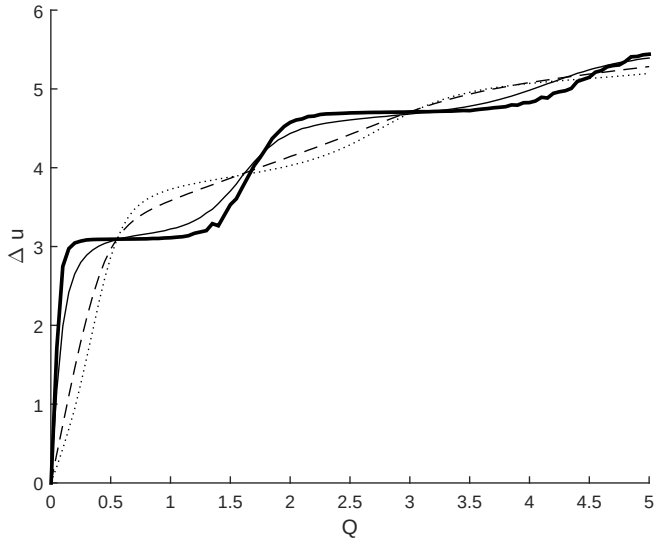

Figure 3.8: Potential difference between walls as a function of the imposed charge for $\gamma = 5$ and $\mu = 1$ (thick), 0.9 (solid), 0.5 (dashed) and 0.3 (dotted).

more than one pair of ions gives a different effect. The difference appears where the plateaus occur, therefore also where the differential capacitance peaks occur. Figure 3.9 shows the differential capacitance for different filling factors. The peaks for μ equals 0.3 appear around the minimum of the completely packed ionic liquid.

Figure 3.10 shows the differential capacitance for $\gamma = 5$ and $\mu = 0.1$. The shift of location where the peaks and plateaus occur, has great effect at the point of zero charge. For a dilute electrolyte the differential capacitance has a peak at $Q = 0$, opposed to the minimum of a packed ionic liquid. The peak at zero charge is significantly smaller than the second peak, however it is still a compelling change in qualitative behaviour.

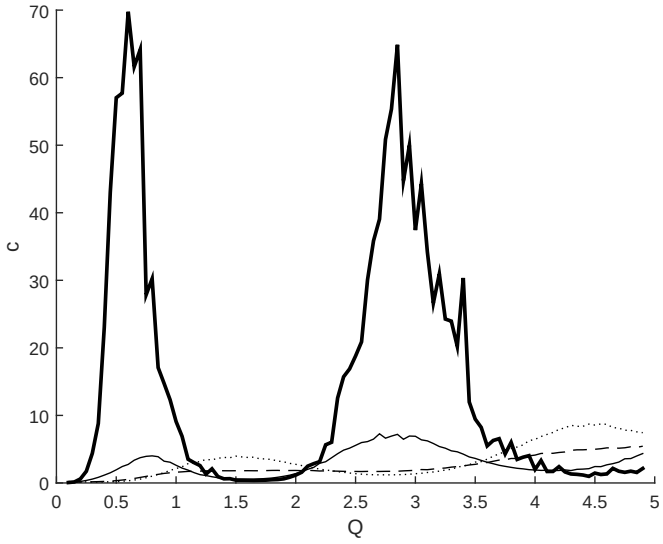

Figure 3.9: Differential capacitance as a function of the imposed charge for $\gamma = 5$ and $\mu = 1$ (thick), 0.9 (solid), 0.5 (dashed) and 0.3 (dotted).

3.6 Effect of Extra Ion-Ion Correlation

Figure 3.11 shows the potential difference as a function of the imposed charge. The dashed and dotted lines include an extra potential in addition to the electrostatic potential, with the strength of ten percent of the electrostatic force between nearest neighbours. The dashed curve represents the system when same charged ions attract each other and different charged ions repulse one another, existing only for nearest neighbours. The opposite is simulated with the dotted curve. Figure 3.12 shows the corresponding differential capacitance. The ion-ion correlation causes the peaks to drastically increase when different ions attract each other. This makes sense as it increases the attracting force between opposite charged ions, which should make the system behave similar to increasing the interaction parameter γ. The opposite happens when same charged ions attract each other.

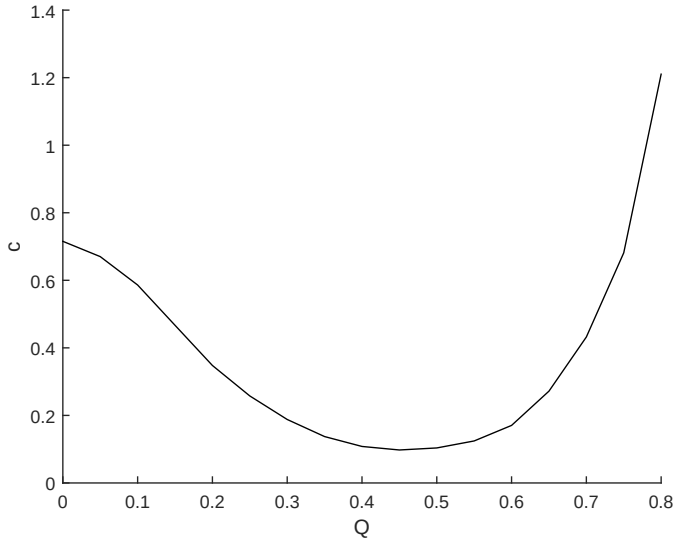

Figure 3.10: Differential capacitance as a function of the imposed charge for $\gamma = 5$ and $\mu = 0.1$.

However, the additional correlation also changes the width and at which imposed charge the plateaus and peaks occur.

The assumed reason for this change is easier explained with figure 3.13. Here the charge oscillations are visualised along the lattice for Q being 1.7. Due to the attraction of like ions the positive ions group up at the boundary. This most likely causes the earlier rise in potential difference seen in figure 3.11. The opposite happens when different ions are attracted to each other. The first ion quickly over-screens the boundary, but to attract two positive ions to the negatively charged boundary it requires much higher imposed charge.

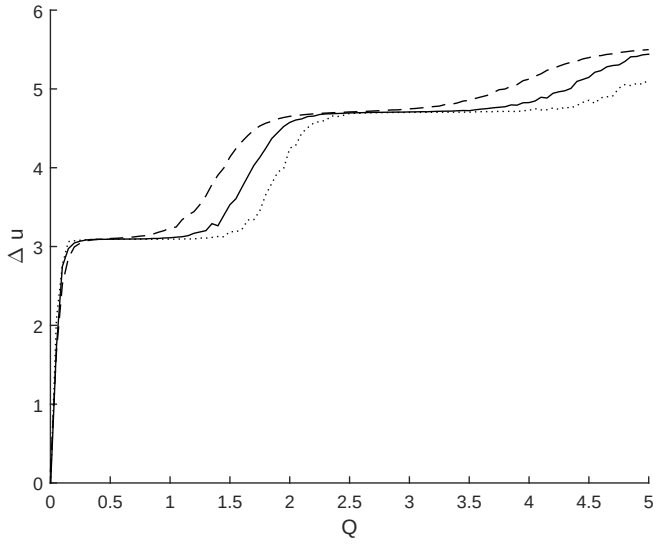

Figure 3.11: Potential difference between walls as a function of the imposed charge for $\gamma = 5$ and extra ion-ion correlation preferring like ions (dashed) and different ions (dotted).

3.7 Screening of Ions

In figure 3.14a the potential difference of the two electrodes is plotted as a function of the imposed charge for screening factor being 0, 0.1, 0.5 and 0.8. As the screening increases, the potential difference decreases. This is expected as the positive ions attracted to the negative surface is screened by negative charges, hence reducing the potential at the boundary. Also, the repeating plateau-like feature disappears with increased screening. The resulting differential capacitance is illustrated in figure 3.14b.

As the ions get screened by the induced charges, the potential energy between the ions is reduced in strength. In figure 3.15a, the potential difference is plotted for screening factor 0.8 and γ being 5, 10 and 20. By scaling up the interaction, the repeating plateau-like feature reappears. Figure 3.15b shows the corresponding

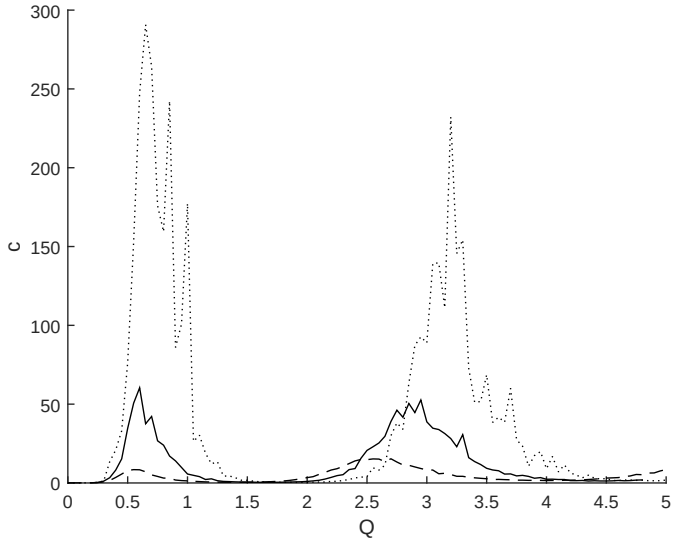

Figure 3.12: Differential capacitance as a function of the imposed charge for $\gamma = 5$ and extra ion-ion correlation preferring like ions (dashed) and different ions (dotted).

differential capacitance. For screening factor 1, figure 3.16a shows the potential difference for the same three γ values mentioned earlier. The repeating plateau-like feature also reappears here, but is not shown as the second plateau requires a higher imposed charge. The resulting differential capacitance is plotted in figure 3.16b. For Q equals five, the screening is so strong that the electrode attracts only one ion to stay by the electrode. With screening factor 0.8, the electrode is about to attract a second ion to stay at the electrode at $Q = 5$. For weak or no screening, it is about to attract a third ion.

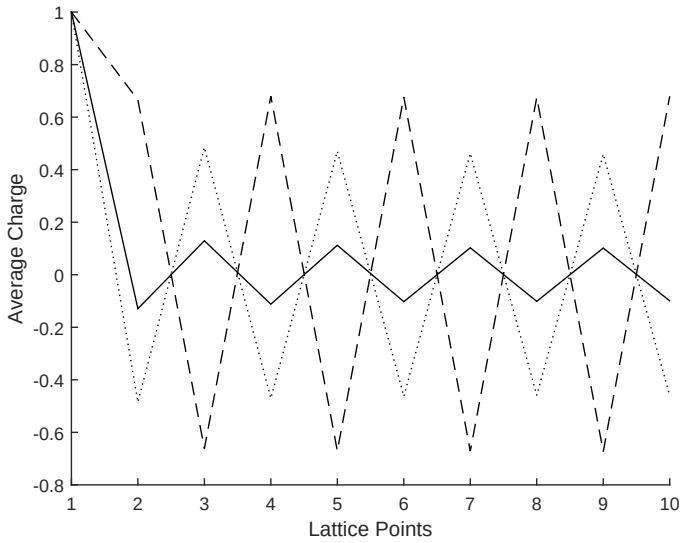

Figure 3.13: Charge oscillations along the lattice for $\gamma = 5$, $Q = 1.7$ and extra ion-ion correlation preferring like ions (dashed), different (dotted) and no preference (solid).

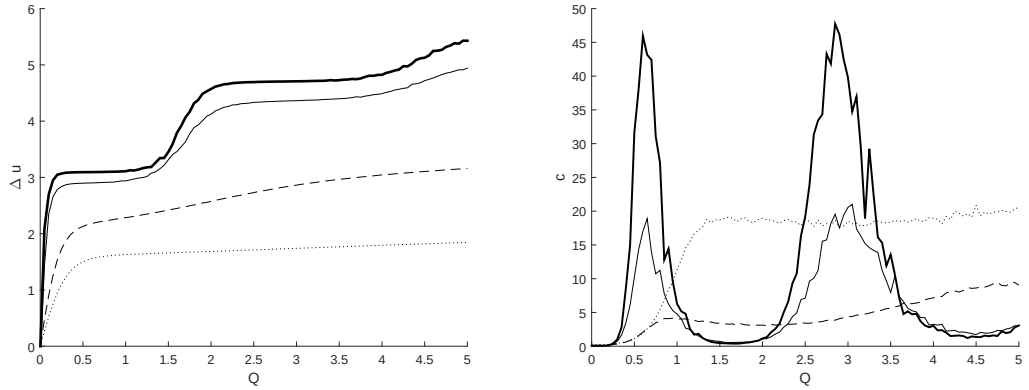

(a) (b)

Figure 3.14: (a) Potential difference between the walls and (b) differential capacitance as a function of the imposed charge for $\gamma = 5$ and screening factor $s = 0$ (thick), 0.1 (solid), 0.5 (dashed) and 0.8 (dotted).

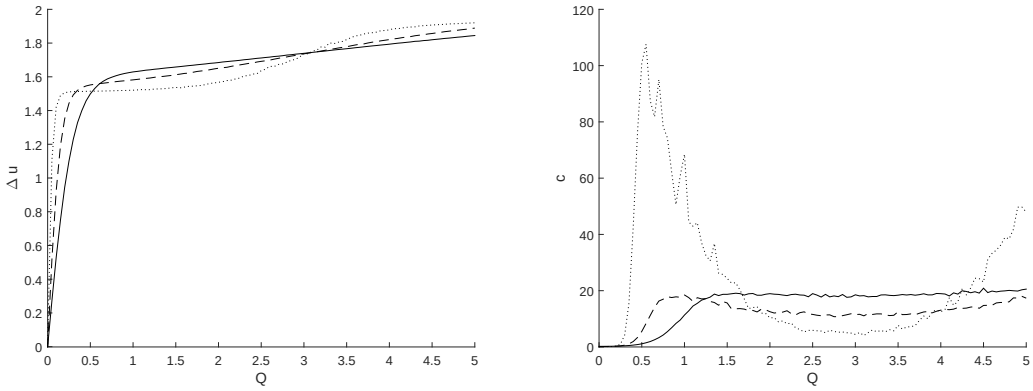

(a) (b)

Figure 3.15: (a) Potential difference between the walls and (b) differential capacitance as a function of the imposed charge for screening factor $s = 0.8$ and $\gamma = 5$ (solid), 10 (dashed) and 20 (dotted).

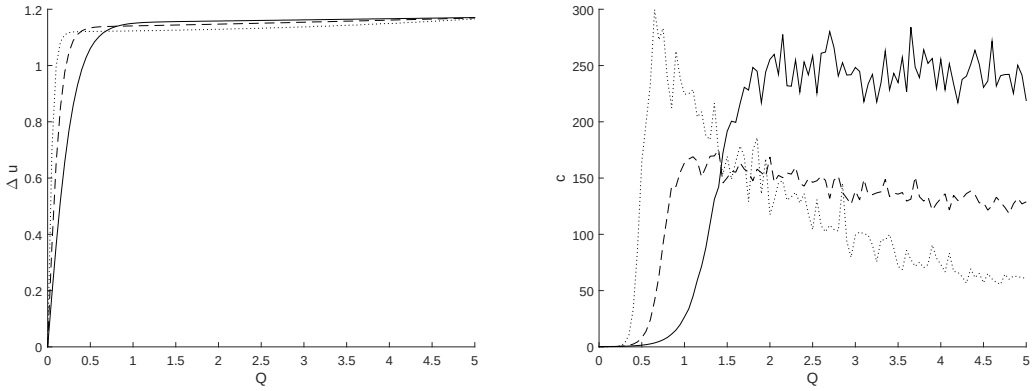

(a) (b)

Figure 3.16: (a) Potential difference between the walls and (b) differential capacitance as a function of the imposed charge for screening factor $s = 1$ and $\gamma = 5$ (solid), 10 (dashed) and 20 (dotted).

Chapter 4

Discussion and Conclusion

In this chapter, the results are discussed in context of existing literature. In the end, a conclusion is drawn along with an outlook for further work.

4.1 Discussion

Considering the convergence of the simulations, one could argue to change the set-up. It would require approximately the same computational power to simulate ten simulations with 10^5 Monte Carlo time steps and one simulation with 10^6 steps. Extrapolating the fitted line from figure 3.1, the error of one simulation of 10^6 steps would be 0.0027. The fitted line of figure 3.1 for 10^5 steps gives an error of 0.0031. The difference is marginal in favour of one simulation of 10^6, but the uncertainty of the fitted lines would probably be higher than the difference of the errors. Nevertheless, the simulations examined in the present work perform well enough as potential difference between the electrodes is of order of one. The fluctuations of the Monte Carlo simulations are the reasons for the spiky behaviour of the differential capacitance curves, but it can be disregarded as the qualitative behaviours are unambiguous.

The model does not behave like the nanopores described in [15]. Instead it behaves like a defect nanopore where the wall along the pore is not properly

connected with the rest of the pore. The pore still keeps the ions confined. A schematic of such a defect pore is illustrated in figure 4.1. The appearance of such a defect nanopore could be caused by impurities in the electrode, preventing charge carriers to move into the pore wall.

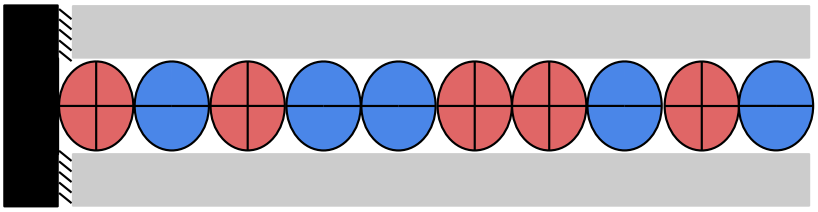

Figure 4.1: Schematic of a defect nanopore.

The properties of the defect pore include overscreening and charge density oscillations, similar to the flat ionic liquid capacitor in [3]. In the flat capacitor, the authors experience perfect screening at integer charges, removing the charge density oscillations. In the defect nanopore, the supposedly perfect screening occurs around 1.5 depending on γ. The difference here might be due to the different interactions as well as that the boundary is half a diameter from the first lattice point.

The potential difference as a function of the imposed charge, as seen in figure 3.6, has a plateau-like behaviour as the temperature decreases. The same plot with a different scaling of the potential is shown in figure 4.2 for the flat capacitor in [3], where they impose charges at the electrodes. The γ is not the same for the two systems. It is hard to compare these, as the exact solution has an oscillation term, causing negative values for the potential difference and the differential capacitance. By comparing the mean field solution and the high temperatures results, one can see that they have a different shape. In the mean field solution, the potential difference increases slowly at low imposed charges and increases more rapidly

at higher imposed charges. For the defect nanopore at high temperatures, the potential difference increases fast at low imposed charges and increases slower at higher imposed charges.

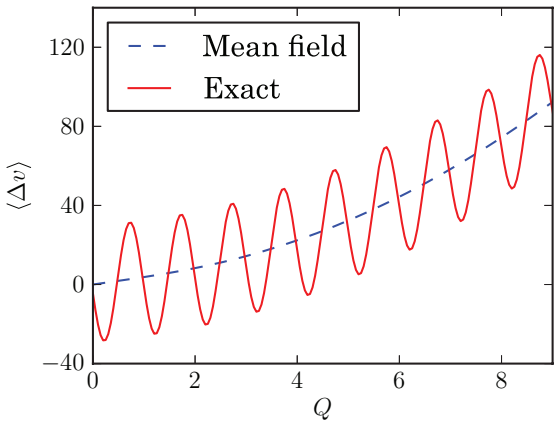

Figure 4.2: Average potential difference as a function of the imposed charge for $\gamma = 1$ and $\mu = 1$ for a flat capacitor. Reprinted with permission from ref. [3]. Copyright 2012, AIP Publishing LLC. Link

Figure 4.3 shows the charges accumulated at the surface of the electrodes as a function of the imposed voltage drop between the electrodes studied in [3]. As ion sheets are replaced with voids and therefore μ decreases, the location of the plateaus changes, similar to the replacement of ions with voids in the defect nanopore shown in figure 3.8. The figures are quite similar, but their axes are flipped, as in the flat capacitor the surface charge is a function of the imposed voltage, opposite to the defect nanopore.

The differential capacitance is calculated as a function of the imposed voltage in this thesis. Most other scientific approaches calculate the differential capacitance as function of the applied potential. Because the potential difference as a function of the imposed charge is a monotonically increasing and one-to-one function, the differential capacitance as a function of potential will have the same

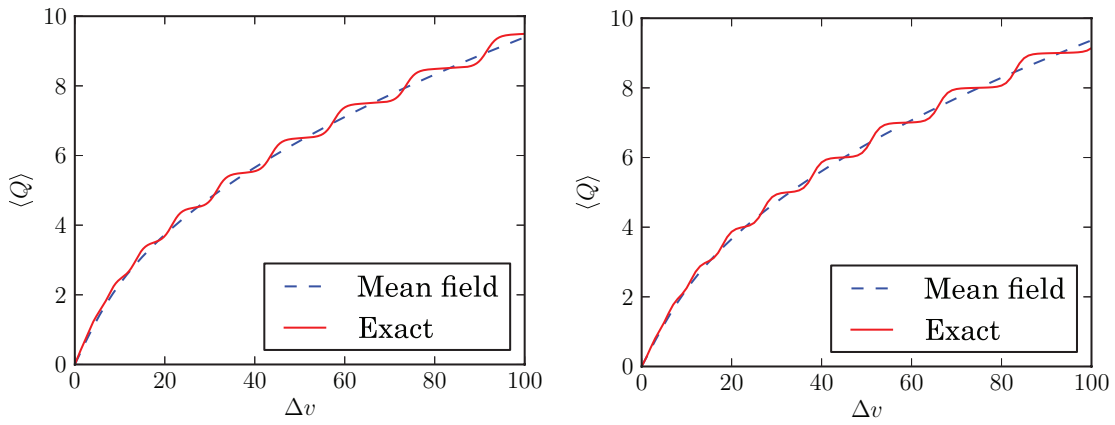

Figure 4.3: Average surface charge as a function of the imposed voltage. $\gamma = 1$ and $\mu = 1$ for left figure and $\gamma = 1$ and $\mu = 0.5$ for right figure. Reprinted with permission from ref. [3]. Copyright 2012, AIP Publishing LLC. Link

qualitative behaviour as a function of the imposed charge. But it will differ in shape. The resulting differential capacitance as a function of potential from γ equals five in figure 3.6 would have thin, sharp peaks at a potential around three and five. The differential capacitance as a function of the imposed charge is seen in figure 3.7, with two broad peaks. The qualitative behaviour of the differential capacitance is the same, making it possible to compare the differential capacitance with existing literature.

A qualitative feature for differential capacitance is whether it has bell-shape or camel-shape around the point of zero charge [35]. For the defect nanopore filled with ionic liquid, the differential capacitance has a camel-shape. However, as the ionic liquid is diluted and ion pairs are replaced with voids or solvent, the differential capacitance has a bell-shape as seen in figure 3.10. For the flat capacitor in [3], when imposing charge at the electrodes results in the mean field solution having a bell shape, opposite to the behaviour of the defect nanopore examined in this study. When they impose a potential drop between the boundaries and

calculate differential capacitance, they also receive a bell-shape. As the sheets of ions are replaced with solvent in the ionic liquid, the differential capacitance has the camel-shape. Both of the systems have oscillations or peaks in the differential capacitance, which are caused by the plateau-like behaviour in figure 3.6 and 4.3 and disappear at high temperatures. The shape around the point of zero charge are opposing for the two systems, assumed to be caused by the different interactions.

For low densities (μ) and imposed charge, the defect pore could be seen as a ionophobic pore. At no imposed charge, the few ions drift around in the pore and when the charges are imposed, the cations move towards the negative charged pore interior and the anions tend towards the positive charge pore interior. This could almost be described as a empty pore beginning to get filled with ions. Around the point of zero charge, it has the bell-shape. In [25], Lee *et al.* study the effect of ionophobic or ionophilic. As the pores become more ionophobic, shown in figure 3 in [25], the differential capacitance starts as a camel-shape and becomes almost a bell-shape. For very ionophilic pore the differential capacitance has a very clear camel-shape, where at low voltages no ions reside inside the pore. The curve has here two peaks, as it must first overcome the ionophilic term, and then the ion-ion correlation. For a neutral and ionophilic pores, it has the camel-shape, similar to the defect nanopore where the pore is with an ionic liquid. The defect nanopore model has the same qualitative behaviour until one ion is fully attracted. After this point the differential capacitance oscillates strongly, because only the interior of the pore is charged and not the whole pore. The camel-shape is also seen for the nanopore Monte Carlo simulation in [24].

Experimental data for differential capacitance for nanopores is presented in figure 4.4 from [4]. Here two different curves are presented, one camel shape

and one bell shaped. The difference between the two is the distribution of pore sizes. Since the pore size in the defect nanopore is only described to be the same size as the ions to keep them confined, not much can be concluded by the experimental data. In addition, the defect nanopores in an electrode are most likely negligible for the capacitance, as most of the charge storage would occur in proper functioning nanopores. If one were to compare the camel-shaped experimental data with the results from the defect nanopore, one would see that the capacitance as a function of the voltage from the results, one would receive a much thinner and sharper peak than the experimental data. This is assumed to be caused by the approximation that ions are hard spheres, when they should be compressible. The simulations by Kondrat *et al.* [4] also has a camel-shape capacitance.

In the models presented in [24] and [25], the screening of ions makes it possible to store more energy in the nanopores. This is because the ion-ion correlation is reduced and it becomes easier to pack same charged ions together. In the defect nanopore, the induced charges reduce the attraction from the inner interior of the pore to the ions as well. This makes it more difficult to store many charges inside the pore. The extra ion-ion correlation makes it easier or harder to store charges in the pore depending on whether it prefers same charged ions to form a group or not. The results from the introduction of extra ion-ion correlation were not considered relevant for the present work, as ion-ion correlation was already included in the model.

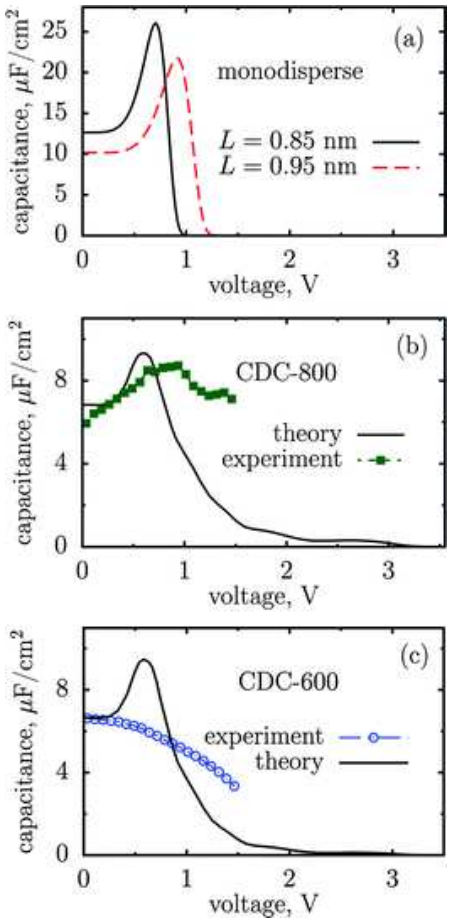

Figure 4.4: (a) Calculated specific differential capacitance as a function of applied voltage for monodisperse pores. (b and c) Calculated capacitance for polydisperse pores is compared with the experimental measured capacitance. The average pore sizes are 0.94 nm (b) and 0.87 nm (c). Reproduced from ref. [4] with permission of The Royal Society of Chemistry. Link

4.2 Conclusion

The main goal of this thesis was to create a simple model for charge storage in a nanopore, and match its qualitative properties to experimental data and existing literature. The resulting model was a model of a defect pore, with its walls along the pore unable to be at same potential as the ends of pore interior. The behaviour of the defect pore was simulated with Monte Carlo simulations. Its properties include overscreening, charge density oscillations and differential capacitance oscillations. All of these disappear at very high temperatures. The differential capacitance of the defect nanopore has the camel-shape, but by replacing ion pairs with voids the differential capacitance has bell-shape. For both cases it would have the opposite shape, if the ions were not contained inside the pore, as the studied flat capacitor. When the pore wall transitioned from insulator to dielectric medium, the induced charges screen both the ion-ion correlation and the effect from the imposed charged at the boundary, making it harder to store same charged ions in the pore.

4.2.1 Outlook

Although the charge storage in defect pores probably is negligible for the total capacitance of an electrode, there could be some interest in finding a method to better predict the behaviour of them. There are a few possible improvements to the model presented in this paper. Since the pore is mirrored, it is only weakly connected to the bulk. When two ions switch places it represents in the real pore that one ion is replaced by the other. If the model is initialised as an ionic liquid with only ions, the model will always be packed, which might not be the case in a nanopore. There should be a way for an ion to leave the pore and go into

the bulk and the other way around. With this integrated into the model one would not need to initialise the pore, but rather decide if the pore is ionophobic or ionophilic and study the effect of those as in [25]. Including the bulk, one might not need the symmetry from mirroring the pore. Without the symmetry, it would be possible to study how the system behaves with different sized and charged ion, which is more realistic for ionic liquids. Another interesting question is how defect nanopores would affect a network of nanopores, and in the end influence the macroscopic capacitance of the capacitor.

Appendix A

Theory Behind the Metropolis Algorithm

Consider calculating averages by selecting phase space points x_i with some probability $P(x_i)$ [34]. By selecting these points, the thermal average from equation (2.12) becomes

$$\bar{A} = \frac{\sum_n exp(-E(n)/k_bT)A(x_i)/P(x_i)}{\sum_n exp(-E(n)/k_bT)/P(x_i)}. \tag{A.1}$$

One would then want $P(x_i)$ to reduce the thermal average equation to

$$\bar{A} = \frac{1}{N}\sum_n A(x_i). \tag{A.2}$$

Metropolis *et al.* [33] then constructed a Markov chain where each state x_{i+1} is constructed from a previous state x_i with a transition probability $T_p(x_i \rightarrow x_{i+1})$. It is possible to choose a T_p that when the length of the Markov chain goes to infinity the distribution function $P(x_i)$ tends towards the equilibrium distribution

$$P_{eq}(x_i) = \frac{exp(-E(x_i)/k_bT)}{\sum_n exp(-E(n)/k_bT)}. \tag{A.3}$$

The principle of detailed balance

$$P_{eq}(x_i)T_p(x_i \to x_{i+1}) = P_{eq}(x_{i+1})T_p(x_{i+1} \to x_i) \tag{A.4}$$

achieves this, giving the transition probabilities the ratio

$$\frac{T_p(x_i \to x_{i+1})}{T_p(x_{i+1} \to x_i)} = \frac{P_{eq}(x_{i+1})}{P_{eq}(x_i)} = exp(\frac{-\Delta E}{k_b T}), \tag{A.5}$$

which the Metropolis Algorithm is a solution of.

Bibliography

[1] J. Chmiola, G. Yushin, Y. Gogotsi, C. Portet, P. Simon, and P. L. Taberna. Anomalous increase in carbon capacitance at pore sizes less than 1 nanometer. *Science*, 313(5794):1760–1763, 2006.

[2] J. Huang, B. G. Sumpter, and V. Meunier. A universal model for nanoporous carbon supercapacitors applicable to diverse pore regimes, carbon materials, and electrolytes. *Chem. Eur. J.*, 14(22):6614–6626, 2008.

[3] V. Démery, D. S. Dean, T. C. Hammant, R. R. Horgan, and R. Podgornik. The one-dimensional coulomb lattice fluid capacitor. *J. Chem. Phys.*, 137(6):064901, 2012.

[4] S. Kondrat, C. R. Perez, V. Presser, Y. Gogotsi, and A. A. Kornyshev. Effect of pore size and its dispersity on the energy storage in nanoporous supercapacitors. *Energ. Environ. Sci.*, 5:6474–6479, 2012.

[5] H. Chen, T. N. Cong, W. Yang, C. Tan, Y. Li, and Y. Ding. Progress in electrical energy storage system: A critical review. *Prog. Nat. Sci.*, 19(3):291–312, 2009.

[6] Y. Ding, Y. Zhao, and G. Yu. A membrane-free ferrocene-based high-rate semiliquid battery. *Nano Lett. Preprint*, 2015.

[7] Z. Yang, J. Zhang, M. C. W. Kintner-Meyer, X. Lu, D. Choi, J. P. Lemmon, and J. Liu. Electrochemical energy storage for green grid. *Chem. Rev.*, 111(5):3577–3613, 2011.

[8] J. R. Miller and P. Simon. Electrochemical capacitors for energy management. *Science*, 321(5889):651–652, 2008.

[9] M. V. Fedorov and A. A. Kornyshev. Ionic liquids at electrified interfaces. *Chem. Rev.*, 114(5):2978–3036, 2014.

[10] D. Andelman in: R. Lipowsky and E. Sackmann. *Handboook of Biological Physics, Volume 1.* Elsevier Science, 1995.

[11] M. Z. Bazant, M. S. Kilic, B. D. Storey, and A. Ajdari. Towards an understanding of induced-charge electrokinetics at large applied voltages in concentrated solutions. *Adv. Colloid Interface Sci.*, 152(1–2):48–88, 2009.

[12] M. Galiński, A. Lewandowski, and I. Stepniak. Ionic liquids as electrolytes. *Electrochim. Acta*, 51(26):5567–5580, 2006.

[13] H. Ohno and K. Fukumoto. Progress in ionic liquids for electrochemical reaction matrices. *Electrochemistry*, 76(1):16–23, 2008.

[14] G. A. Snook, P. Kao, and A. S. Best. Conducting-polymer-based supercapacitor devices and electrodes. *J. of Power Sources*, 196(1):1–12, 2011.

[15] P. Simon and Y. Gogotsi. Charge storage mechanism in nanoporous carbons and its consequence for electrical double layer capacitors. *Philos. T. Roy. Soc. A*, 368(1923):3457–3467, 2010.

[16] G. Wang, L. Zhang, and J. Zhang. A review of electrode materials for electrochemical supercapacitors. *Chem. Soc. Rev.*, 41:797–828, 2012.

[17] C. Largeot, C. Portet, J. Chmiola, P. L. Taberna, Y. Gogotsi, and P. Simon. Relation between the ion size and pore size for an electric double-layer capacitor. *J. Am. Chem. Soc.*, 130(9):2730–2731, 2008.

[18] R. Lin, P. Huang, J. Ségalini, C. Largeot, P.L. Taberna, J. Chmiola, Y. Gogotsi, and P. Simon. Solvent effect on the ion adsorption from ionic liquid electrolyte into sub-nanometer carbon pores. *Electrochim. Acta*, 54(27):7025–7032, 2009.

[19] D. Jiang, Z. Jin, and J. Wu. Oscillation of capacitance inside nanopores. *Nano Lett.*, 11(12):5373–5377, 2011.

[20] P. Wu, J. Huang, V. Meunier, B. G. Sumpter, and R. Qiao. Complex capacitance scaling in ionic liquids-filled nanopores. *ACS Nano*, 5(11):9044–9051, 2011.

[21] G. Feng and P. T. Cummings. Supercapacitor capacitance exhibits oscillatory behavior as a function of nanopore size. *J. Phys. Chem. Lett.*, 2(22):2859–2864, 2011.

[22] J. Huang, B. G. Sumpter, and V. Meunier. Theoretical model for nanoporous carbon supercapacitors. *Angew. Chem. Int. Ed.*, 47(3):520–524, 2008.

[23] B. Skinner, M. S. Loth, and B. I. Shklovskii. Capacitance of the double layer formed at the metal/ionic-conductor interface: How large can it be? *Phys. Rev. Lett.*, 104:128302, 2010.

[24] B. Skinner, T. Chen, M. S. Loth, and B. I. Shklovskii. Theory of volumetric capacitance of an electric double-layer supercapacitor. *Phys. Rev. E*, 83:056102, 2011.

[25] A. A. Lee, S. Kondrat, and A. A. Kornyshev. Single-file charge storage in conducting nanopores. *Phys. Rev. Lett.*, 113, 2014.

[26] S. Kondrat and A. Kornyshev. Superionic state in double-layer capacitors with nanoporous electrodes. *J. Phys. Condens. Mat.*, 23(2):022201, 2011.

[27] Y. He, J. Huang, B. G. Sumpter, A. A. Kornyshev, and R. Qiao. Dynamic charge storage in ionic liquids-filled nanopores: Insight from a computational cyclic voltammetry study. *J. Phys. Chem. Lett.*, 6(1):22–30, 2015.

[28] S. Kondrat, P. Wu, R. Qiao, and A. A. Kornyshev. Accelerating charging dynamics in subnanometre pores. *Nat. Mater.*, 13(4):387–393, 2014.

[29] H. Kano, H. Fujioka, and C. F. Martin. Optimal smoothing and interpolating splines with constraints. *Appl. Math. and Comput.*, 218(5):1831–1844, 2011.

[30] B. D. Storey and M. Z. Bazant. Effects of electrostatic correlations on electrokinetic phenomena. *Phys. Rev. E*, 86:056303, 2012.

[31] M. Z. Bazant, B. D. Storey, and A. A. Kornyshev. Double layer in ionic liquids: Overscreening versus crowding. *Phys. Rev. Lett.*, 106:046102, 2011.

[32] D. Yoshioka. *Statistical Physics*. Springer, 2007.

[33] N. Metropolis, A. W. Rosenbluth, M. N. Rosenbluth, A. H. Teller, and E. Teller. Equation of state calculations by fast computing machines. *J. Chem. Phys.*, 21(6):1087–1092, 1953.

[34] K. Binder and D. W. Heermann. *Monte Carlo Simulation in Statistical Physics*. Springer, 5th edition, 2010.

[35] A. A. Kornyshev. Double-layer in ionic liquids: Paradigm change? *J. Phys. Chem. B*, 111(20):5545–5557, 2007.